HONIR: an optical and near-infrared simultaneous imager, spectrograph, and polarimeter for the 1.5-m Kanata telescope

Hiroshi Akitaya[a], Yuki Moritani[a], Takahiro Ui[a], Takeshi Urano[b], Yuma Ohashi[b], Koji S. Kawabata[a], Asami Nakashima[c], Mahito Sasada[d], Kiyoshi Sakimoto[b], Tatsuya Harao[b], Hisashi Miyamoto[e], Risako Matsui[b], Ryosuke Itoh[b], Katsutoshi Takaki[b], Issei Ueno[b], Takashi Ohsugi[a,b], Hidehiko Nakaya[f], Takuya Yamashita[f], and Michitoshi Yoshida[a]

[a]Hiroshima Astrophysical Science Center, Hiroshima University, Kagamiyama 1-3-1, Higashi-Hiroshima 739-8526, JAPAN;
[b]Department of Physical Science, School of Science, Hiroshima University, Kagamiyama 1-3-1, Higashi-Hiroshima 739-8526, JAPAN;
[c]Nagoya City Science Museum, 17-1, Sakae 2-chome, Naka-ku, Nagoya 460-0008, JAPAN;
[d]Department of Astronomy, Kyoto University, Kitashirakawa-Oiwake-cho, Sakyo-ku, Kyoto 606-8502, JAPAN;
[e]Molex Japan Co., Ltd., Fukami-Higashi 1-5-4, Yamato, Kanagawa 242-8585, JAPAN;
[f]National Astronomical Observatory of Japan, Osawa 2-21-1, Mitaka, Tokyo 181-8588, JAPAN

ABSTRACT

We have developed an optical and near-infrared instrument HONIR (Hiroshima Optical and Near-InfraRed camera) with imaging, spectroscopy, and polarimetry capabilities in two (one optical and one near-infrared) bands simultaneously. Imaging capability with a field of view of 10 arcmin by 10 arcmin has been available since 2011, as reported in the previous SPIE conference. In addition, spectroscopic and polarimetric optical components (grisms, an Wollaston prism, a half-wave plate, and focal masks) were installed in the instrument, which enabled us to perform spectroscopy and linear polarization measurement by imaging polarimetry and spectro-polarimetry. Spectral resolution of $R = \lambda/\Delta\lambda \sim 440 - 800$ is achieved in spectroscopy using a slit mask with an $1''.3$ width. In polarimetry, instrumental polarization is less than ~ 0.05 % with stability of better than ~ 0.05 %, which is sufficiently small to achieve an aimed accuracy of polarization measurement of ~ 0.1 % at primal observing wavelengths.

1. INTRODUCTION

HONIR (Hiroshima Optical and Near-InfraRed camera) is an optical and near-infrared simultaneous imager, spectrometer, and polarimeter attached at the Cassegrain focus of the 1.5-m Kanata telescope at Higashi-hiroshima Observatory (Hiroshima, Japan) operated by Hiroshima Astrophysical Science Center, Hiroshima University (Fig. 1).

We had accomplished many observational results on variable or transient objects, such as blazers,[1–3] supernovae,[4] young stellar objects, and so on, by use of the optical and near-infrared simultaneous instrument TRISPEC,[5] which is capable of imaging, spectroscopy, and polarimetry, since 2006. To improve the research activity, we planned developing a new instrument HONIR with much higher sensitivity and spacial resolution than TRISPEC.

We began developing HONIR in 2007. The optical and near-infrared simultaneous imaging capability (Fig. 2) was introduced in 2011 as reported in the previous SPIE conference.[6] In addition, we installed a

Further author information: (Send correspondence to H. Akitaya)
H. Akitaya : E-mail: akitaya@hiroshima-u.ac.jp, Telephone: +81 82 424 5765, Fax: +81 82 424 5765

function of spectroscopy in 2013. A polarimetric function, which enables us to perform imaging polarimetry and spectro-polarimetry for linear polarization, in combination with an imaging function or a spectroscopy function in existence, was installed in early 2014.

We describe basic design and specifications of HONIR in Section 2. Details of the imaging capability, spectroscopic capability, and polarimetric capability are described in Section 3, 4, and 5, respectively. We summarize current status of HONIR and mention future prospects in Section 6.

2. BASIC DESIGN AND SPECIFICATIONS OF HONIR

Optical design of HONIR is shown in Fig. 3. Principal optical components of HONIR, except for a mechanical shutter and a half-wave plate for polarimetry, are placed on an optical bench cooled down to $\sim$ 65 K in a vacuum chamber. An incident ray from the telescope is once focused at the telescope focal plane in the chamber, followed by a collimator lens and a cold stop at the exit pupil plane of the telescope. A following dichroic mirror splits the ray into a folded optical ray ("Optical Arm"; 0.5–1.0 μm) and a forthright near-infrared ray ("IR Arm #1"; 1.15–2.4 μm). Focal images are finally focused on an optical CCD detector and

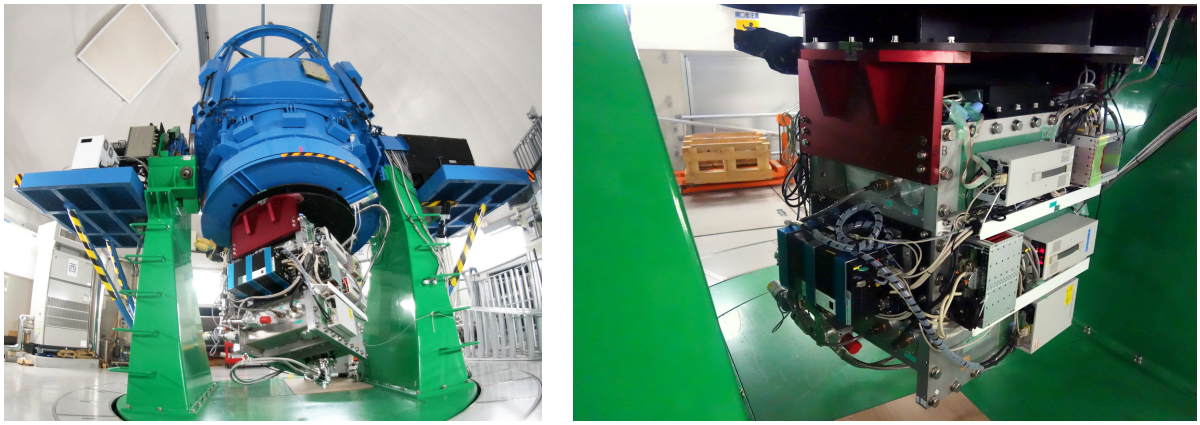

Figure 1. HONIR attached on the Kanata Telescope.

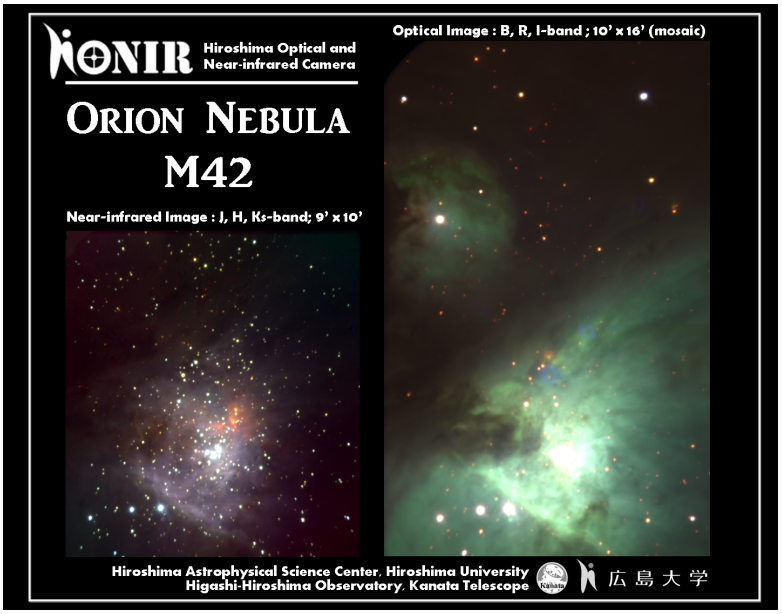

Figure 2. Optical and near-infrared imaging observation of M42 (RGB pseudo color).

a near-infrared HgCdTe VIRGO-2K detector separately by a camera lens in each arm after passing through a band-pass filter and/or a grism.

HONIR is equipped with six rotating turrets to insert arbitrary optical components into the optical train. A focal mask turret (Turret #1) provides the telescope focal plane with one of aperture masks or slit masks for imaging, spectroscopy, polarimetry, or experimental measurements (e.g. a pinhole mask). A pupil mask turret (Turret #2) at the pupil plane contains a cold stop with a diameter of 26 mm for imaging observation, an Wollaston prism for polarimetry, and some masks for experiments. Each arm after split by the dichroic mirror has two turrets (Turret #3 and #4 for the IR Arm #1, and #5 and #6 for the Optical Arm). They contain band-pass filters (in the turret #4 and #6) and grisms (#3 and #5). Each turret is rotated by a stepping motor controlled by the integrated control system *Motionnet* (Nippon Pulse Motor Co., Ltd.).

The detector in the Optical Arm is a fully-depleted back-illuminated CCD array with 2048 × 4096 pixels with a pixel size of 15 μm (Hamamatsu Photonics K. K.,), which is controlled by the *Messia 5*[7] and *MFront 2*[8,9] systems. An image is read at a frame rate of 17.4 sec/frame with a readout noise of ~ 4 e^-/pixel at a gain of 2.7 e^-/ADU.

For the IR Arm #1, a HgCdTe VIRGO-2K array with 2048 × 2048 pixels (20 μm pixel size) controlled by the *Messia 5* and *MACS2*[10] systems is used. A full image area of the detector is read at a frame rate of 4.5 sec/frame via four readout ports in parallel at a readout noise of ~ 24 e^-/pixel at a gain of 11.6 e^-/ADU. We are currently developing a new readout system for the VIRGO-2K array, based on design of the Kiso Control Array,[11] aiming to read a whole image at ~ 1.2 sec/frame via 16 readout ports in parallel with a smaller readout noise.[12]

Our design leaves room for appending an extra infra-red arm (IR Arm #2; see the upper part of Fig. 3(a)), which consists of an additional dichroic mirror that folds the incident near-infrared ray in the existing IR Arm #1 with wavelengths of 1.15-1.35 μm (J band), a pair of a filter and grism turrets, a camera lens, and an extra infra-red detector. A function of simultaneous observation in three bands (optical, J, and H–K bands) will be achieved in consequence.

Basic specifications of HONIR is summarized in Table 1. Details of the basic optics, cryostat, mechatronics, and readout systems for the detectors are also described in the previous conference paper on this instrument.[6]

(a) (b)

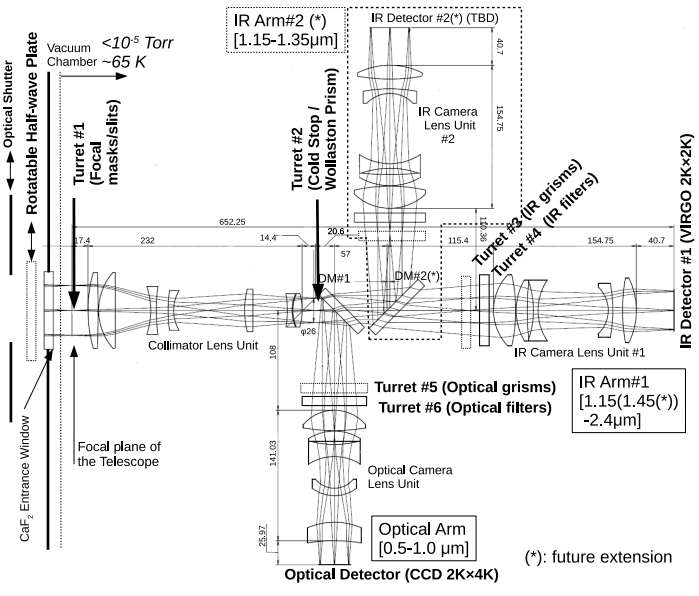

Figure 3. (a) Optical layout of HONIR and (b) components in the vacuum chamber.

Table 1. Basic specifications of HONIR.

Property		Arm	
		Optical	IR Arm #1[a]
Wavelength coverage (μm)		0.5[b]1.0	1.15–2.40
Field of view (FoV) (arcmin)		10×10	10×10
Plate scale (arcsec/mm)[c]		11.148	
Size of the whole FoV (mm)[c]		53.8×53.8	
Sampling rate (arcsec/pix)		0.294	0.295
Size of the whole imaging area (mm)[d]		30.7×30.7	40.9×40.9
Filters		B,[b] V, R_C, I_C, Y	Y, J, H, K_s
		$< 0.58\,\mu$m cut filter	$< 1.33\,\mu$m cut filter
Spectroscopy	Slits	$1''.3$ (0.12 mm), $2''.2$ (0.2 mm), $6''$ (0.54 mm)	
	Grisms	BK7; 300 gr/mm (*Optical*)	BK7; 180 gr/mm (*IR-short*), S-FTM16; 120 gr/mm (*IR-long*)
Polarimetry	Masks	$9'.7 \times 0'.75 \times 5$ slots, $2''.2 \times 45'' \times 5$ slits	
	Analyzer	YLF Wollaston prism	
	Modulator	Pancharatnam type super-achromatic half-wave plate	
Detector	Type	CCD	HgCdTe VIRGO-2K
	Vendor	Hamamatsu Photonics	Raytheon
	Format (pixels)	2048×4096	2048×2048
	Pitch (μm)	15	20
	Size (mm)	30.72×61.44	40.96×40.96

[a] To be divided into the IR Arm #2 for 1.15–1.35 μm and the IR Arm #1 for 1.45–2.40 μm when another arm will be installed in future.
[b] Partially transparent at 0.4–0.5 μm (B band).
[c] At the telescope focal plane.
[d] On the detector.

3. IMAGING OBSERVATION

Imaging observation is performed by inserting a focal mask with a square aperture with 10 arcmin by 10 arcmin and band-pass filters in the optical trains. Images with a field of view of 10 arcmin by 10 arcmin at an optical and near-infrared bands are simultaneously focused on the CCD detector and the HgCdTe detector, respectively. A pixel scale is 0.294 arcsec/pix on the optical CCD detector, and 0.295 arcsec/pix on the near-infrared HgCdTe detector.

4. SPECTROSCOPY

Spectroscopy of HONIR is performed by inserting a focal slit mask at the telescope focal plane and a grism into each optical train after split by the dichroic mirror.

Three types of focal slit masks made from aluminum alloy are used for spectroscopy: a $2''.2$ (0.20 mm) width slit for $R \sim 350$ (when used with the nominal grisms), an $1''.3$ (0.12 mm) width slit for $R \sim 600$, and a $6''$ (0.54 mm) width slit for spectro-photometry (Fig. 4(a)). Every slit has a length of $9'.7$ (52 mm).

Three grisms have been installed in the grism turrets (Table 2, Fig. 4(b)-(d)).

A BK7 "Optical" grism is used at the Optical Arm, which covers the entire optical wavelengths between 0.45 and 1.1 μm. A BK7 "IR-short" grism and a S-FTM16 "IR-long" grism are alternatively used at the IR #1 Arm, covering 0.95–1.53 μm (Y, J, and partial H bands) and 1.15–2.38 μm (partial J, H, and K bands), respectively (Fig. 5). To suppresses contamination of secondary diffracted rays, combine use of an order sorting filter, a 0.58 μm cut filter for the Optical grism and an 1.33 μm cut filter for the IR-long grism, is also possible.

Table 2. Specifications of the grisms.

Name	Optical	IR-short	IR-long
Arm	Optical	IR #1	
Wavelength coverage on the detector	0.58(0.45[a])–1.1	0.95–1.43	1.33(1.15[a])–2.38
Wavelength of the maximum efficiency (μm)	0.683	1.232	1.933
Material	BK7	BK7	S-FTM16
Wedge angle (degrees)	21.5	23.5	22.5
Grooves (gr/mm)	300	180	120
Blaze angle (degrees)	23.0	23.9	26.7
Groove pattern type[b]	54-039R	54-870R	54-831R
Size (mm)	51 × 51× 21	59 × 59 × 27	59 × 59 × 26
Effective diameter (mm)	47	55	55

[a] Without an order sorting filter.
[b] Model number of Richardson Gratings, Newport Corporation.

Throughput of spectroscopy, including reflectance of the telescope mirrors, is about $\sim 15-20$ % at the major wavelength ranges.

Actual wavelength resolution ($R = \lambda/\Delta\lambda$) was evaluated by measuring line widths of emission lines of arc lamps (Fig. 6). When using the $1''.3$ slit, $R \sim 440$ (V band)–800 (z' band) with the Optical grism, ~ 630 (J band) with the IR-short grism, and ~ 570 (H band)–440 (K_s band) with the IR-long grism are achieved.

An example of spectroscopic observation of a celestial object is shown in Fig. 7.

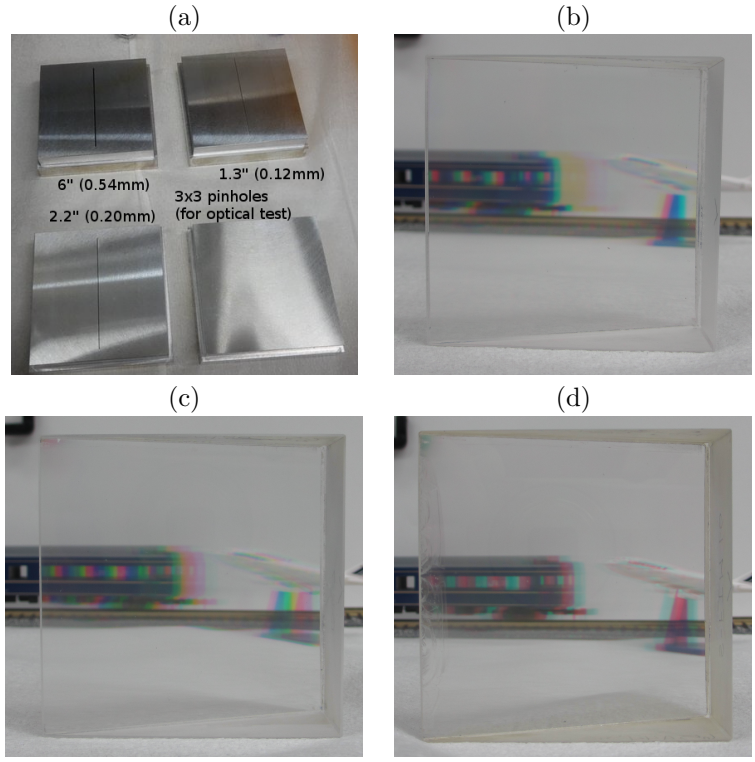

Figure 4. Pictures of (a) the slit masks, (b) the Optical grism, (c) the IR-short grism, and (d) the IR-long grism.

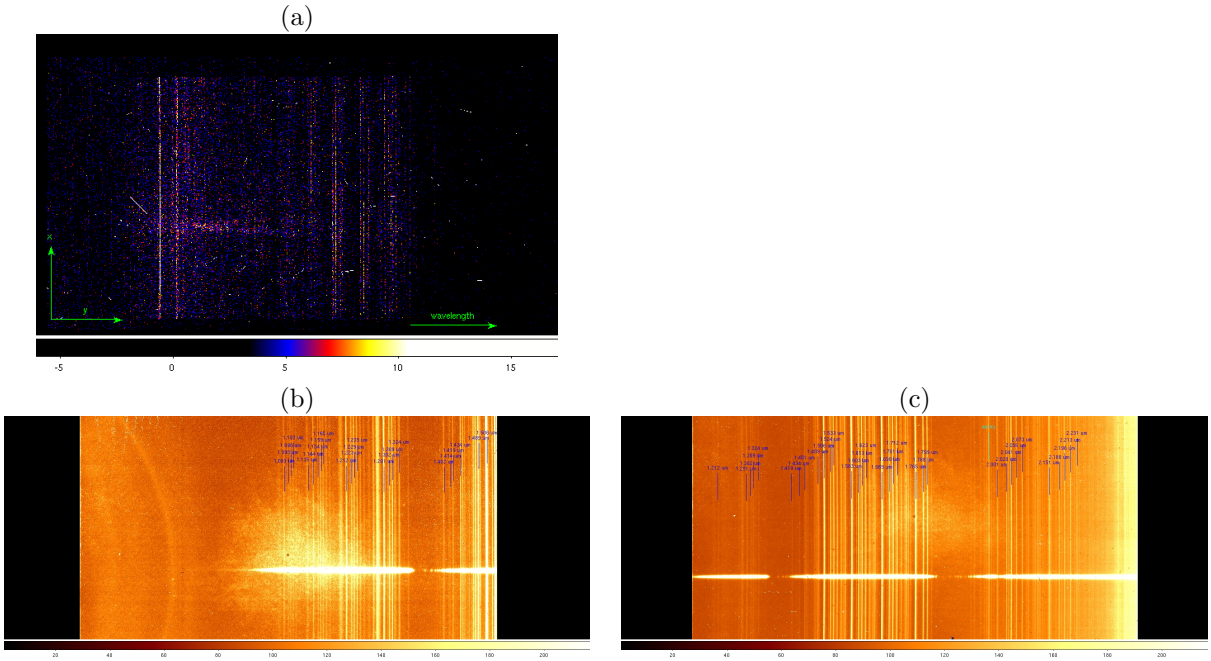

Figure 5. Image samples of spectroscopy of sky emission lines by (a) the Optical grism, (b) the IR-short grism, and (c) the IR-long grism.

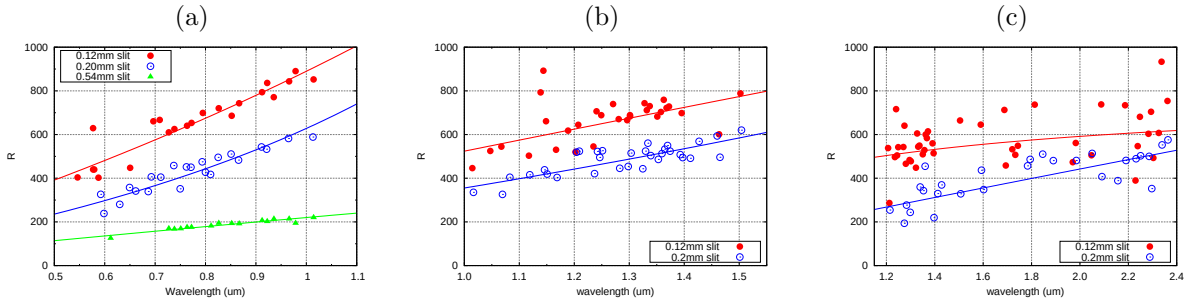

Figure 6. Spectral resolution measured from emission lines of arc lamps with (a) the Optical grism, (b) the IR-short grism, and (c) the IR-long grism.

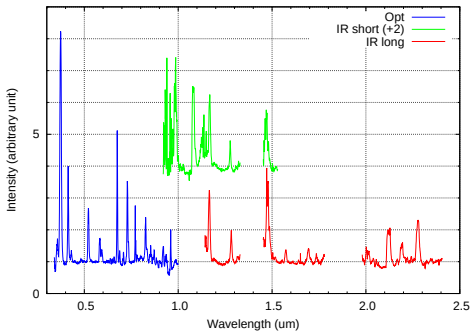

Figure 7. Spectroscopy of an Wolf-Rayet star WR006 with the 1″.3 mm slit normalized at the continuum level.

5. POLARIMETRY

HONIR is equipped with an Wollaston prism, a rotatable super-achromatic half-wave plate, and focal masks, to perform linear polarization measurement.

5.1 Wollaston prism

An Wollaston prism is inserted at the pupil of the optical train to split the incident ray into a pair of linear polarized rays (an ordinary ray (o-ray) and extraordinary ray (e-ray)) orthogonally polarized each other, which are focused on the detectors separately.

We selected $LiYF_4$ (YLF) as the material of the Wollaston prism after comparison with other materials. Physical parameters of YLF and other materials are summarized in Table 3. The YLF satisfies the following requirements: (1) enough transparency between 0.5 and 2.5 μm ($\lambda_{\rm trans}$), (2) large birefringence to achieve a large separation angle between o- and e-rays (large Δn), (3) small color dispersion of a separation angle to suppress chromatic aberration of a stellar image with a broad-band filter (small V), (4) small difference between coefficients of linear thermal expansion of each birefringent axis (small $\Delta\alpha$) to avoid thermal destruction of the prism and divorce of optical contact during thermal cycles, and (5) past experiences using at a cryogenic temperature ($\sim$ 85 K).[13]

The Wollaston prism consists of two wedged YLF prisms with an wedge angle of 16°.39 optically contacted to one another with their fast axes orthogonally directed. It measures 34 mm by 34 mm with a height of 12 mm. An effective aperture diameter is 30 mm. The Wollaston prism was manufactured by Nitto Optical Co., Ltd. Its picture and drawing are shown in Fig. 8.

A separation angle between the split beams, slightly varying with wavelength, is 0°.7685 at 0.47 μm and 0°.7381 at 2.4 μm, corresponding to 47.8 arcsec and 45.9 arcsec in a celestial angular scale projected on the detectors, respectively. For V-band imaging polarimetry, at which color dispersion becomes the largest, image elongation by color dispersion of the Wollaston prism is $\sim$ 0.30 arcsec, sufficiently smaller than the typical seeing size of $\sim$1–2 arcsec.

5.2 Rotatable half-wave plate (HWP)

As a modulator, a rotatable half-wave plate (HWP) is inserted in front of the optical window of the cold chamber followed by a focal mask only when polarimetry is performed. A position angle of linear polarization of the incident ray from the telescope is rotated relative to the instrument according to the variable position angle of the HWP.

The HWP is a Pancharatnam type super-achromatic half-wave plate consisting of three pairs of an SiO_2 and MgF_2 layers finally covered with anhydrous silica plates on the top and bottom. Specifications of the HWP are summarized in Table 4.

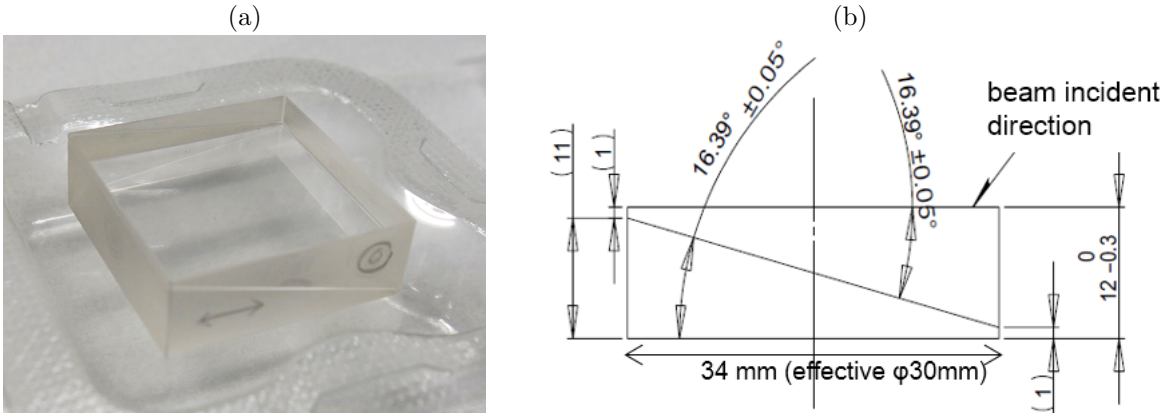

Figure 8. (a) The YLF Wollaston prism and (b) design of the prism.

.

Table 3. Comparison of candidate materials for the Wollaston prism.

Material	$\lambda_{\rm trans}$[a](μm)	$n_{\rm o}$[b]	Δn [c]	$\lambda_{\Delta n}$[c](μm)	V[d](0.6 μm)	V[d](2.2 μm)	$\Delta\alpha$[e]($\times 10^{-6}$)
Calcite	0.21–2.1	1.66	-0.17	0.633	22	36	18.7
$\alpha-$BBO	0.19–2.1	1.67	-0.12	0.532	30	33	-32
YVO_4	0.45–3.4	1.9929	0.2225	1.55	11	547	-6.9
$LiNbO_3$	0.50–3.8	2.146	0.074	1.3	8	67	-14.7
Rutile	0.55-4.3	2.454	0.256	1.5296	15	-29	-2.7
$LiYF_4$ (YLF)	0.30-4.0	1.44845	0.02218	1.0	43	-264	3
MgF_2	0.13–7.0	1.37713	0.01176	0.6234	71	115	5.2
SiO_2	0.20–2.4	1.54	0.009	0.633	31	45	?

[a] Transparent wavelength range.
[b] Refractive index for an ordinary ray.
[c] Birefringence. $\Delta n = n_{\rm e} - n_{\rm o}$ at a wavelength $\lambda_{\Delta n}$.
[d] Color dispersion of a split ray. $V(\lambda) = \Delta n(\lambda)/\left[\Delta n(\lambda - 0.1\,\mu{\rm m}) - \Delta n(\lambda + 0.1\mu{\rm m})\right]$.
[e] Difference between coefficients of thermal expansion of two orthogonal optical axes.

Table 4. Specifications of the half-wave plate.

Type	Pancharatnam type super-achromatic
Size	ϕ 100 mm, 9.6 mm thick
Effective aperture	ϕ 92 mm
Wavefront error (at 633 nm)	$\lambda/10$
Retardance (at 450–2300 nm)	$180^\circ \pm 9^\circ$
Transmittance (at 450-2300 nm)	$>$ 90 % ($>$ 80 % at $>$ 2,200 nm)
Manufacturer	Kogakugiken Corp. (Japan)

The HWP is mounted in a circular cell supported by a crossed roller bearing (CRA13008CC0; THK Co., Ltd.) on a base plate. The cell is rotated with a 2-phase stepping motor (PK243DA; Oriental Motor Co., Ltd.) on which a backlush-free gear (NS50SU 60B + 0505; Kyoiku Gear MFG Co., Ltd.) is attached. The rotating unit is mounted on linear slide guides and moved with a ball screw driven with a 5-phase stepping motor with an electromagnetic brake (RKS544MA; Oriental Motor Co., Ltd.). Fiducial position angles of the HWP cell and limit positions of the slide unit are detected by photointerrupters (EE-SX3088; Omron Corp.). A positioning accuracy of a HWP position angle is better than $0^\circ.05$.

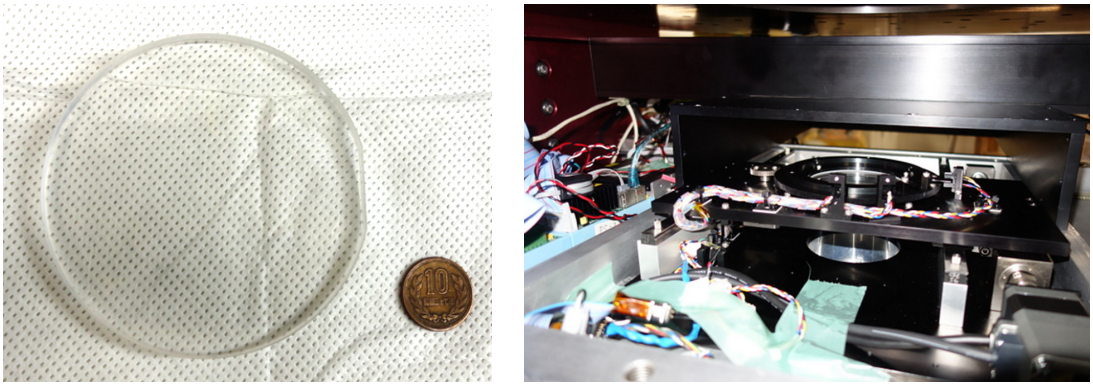

(a) (b)

Figure 9. (a) The half-wave plate and (b) the rotation unit mounted on HONIR.

5.3 Focal masks for polarimetry

A focal mask with discrete rectangular slots or slits are used for polarimetry. For imaging polarimetry, a mask with five discrete rectangular slots with a size of $9'.7$ by $0'.75$ (52 mm by 4 mm in actual scale on the focal plane) at every $15'$ (8.4 mm) is used. For spectro-polarimetry, five discrete slits with a $2''.2$ (0.2 mm) width and $45''$ (4.0 mm) length at every $15'$ (8.4 mm) is used (Fig. 10(a)(b)). Thus, o-ray and e-ray images or spectra are focused on a detector without their overlapping.

Considering the worries about unexpected polarization generation at aperture edges, machinable ceramic (MACELITE HSP black by Ariake Materials Co., Ltd.), not metal material, is used as a base of the masks. Every edge of the apertures was carved very sharply (Fig. 10(c)).

Five pairs of an o-ray and e-ray images or spectra are focused on the optical and infrared detectors (Fig. 11). Spectral resolution of spectro-polarimetry is $R \sim 200-600$, the same as that of spectrometry with a $2''.2$ slit (Section 4).

5.4 Measurement of linear polarization

Normalized stokes parameters $q = Q/I$ and $u = U/I$, or a polarization degree p and a position angle θ, are derived from four pairs of observed intensity signals of an o-ray and e-ray of images or spectra obtained at four half-wave plate position angles of $\psi = 0°.0$, $45°.0$, $22°.5$, and $67°.5$ using the formulae[14]

$$q(\lambda) = \frac{1 - a_{\rm Q}(\lambda)}{1 + a_{\rm Q}(\lambda)}, \qquad u(\lambda) = \frac{1 - a_{\rm U}(\lambda)}{1 + a_{\rm U}(\lambda)}, \tag{1}$$

$$a_{\rm Q}(\lambda) = \sqrt{\frac{\kappa(\lambda, 0°.0)}{\kappa(\lambda, 45°.0)}}, \qquad a_{\rm U}(\lambda) = \sqrt{\frac{\kappa(\lambda, 22°.5)}{\kappa(\lambda, 67°.5)}}, \tag{2}$$

$$\kappa(\lambda, \psi) = \frac{I_{\rm e(obs)}(\lambda, \psi)}{I_{\rm o(obs)}(\lambda, \psi)}, \tag{3}$$

and

$$p(\lambda) = \sqrt{q(\lambda)^2 + u(\lambda)^2}, \qquad \theta(\lambda) = \frac{1}{2}{\rm atan}\left(\frac{u(\lambda)}{q(\lambda)}\right), \tag{4}$$

where $I_{\rm o(obs)}(\lambda, \psi)$ and $I_{\rm e(obs)}(\lambda, \psi)$ are observed signals of an o-ray and e-ray, at a wavelength λ and a position angle of the HWP ψ, respectively. Using these formulae, difference of transmittance efficiencies between an

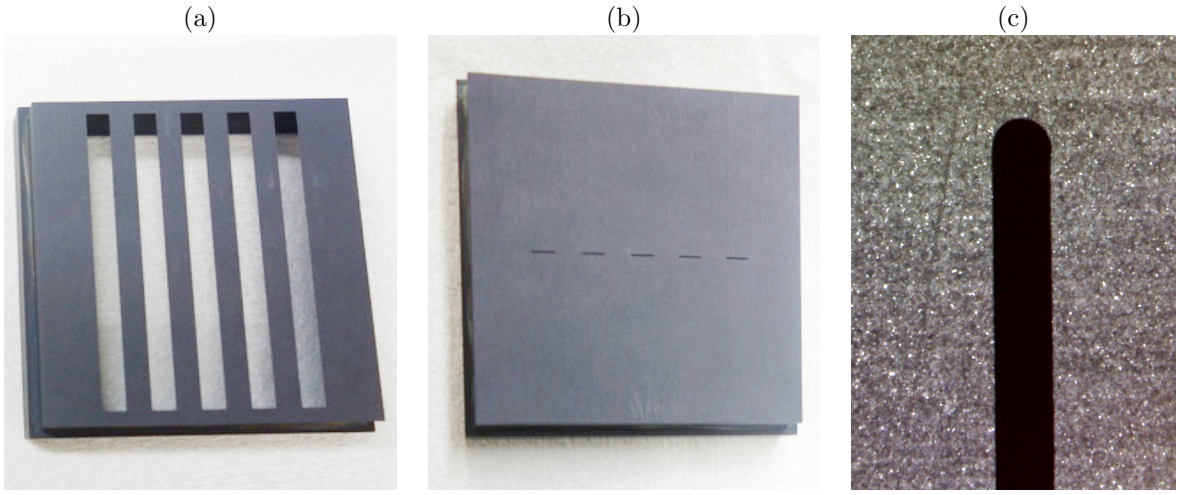

Figure 10. Focal masks for (a) imaging polarimetry and (b) spectro-polarimetry. (c) Magnification of a slit edge of the spectro-polarimetry mask.

o-ray and e-ray in the instrument, and variation of terrestrial atmospheric transmittance between a pair of distinct exposures (ψ = 0°.0 and 45°.0 for q measurement, or 22°.5 and 45°.0 for u measurement) are completely cancelled out.

5.5 Polarimetric performance

We aim at achieving an accuracy of linear polarization measurement less than 0.1 % to detect typically small celestial polarization signals of the order of a few percent or less. Small instrumental polarization with small fluctuation, which is expected by operating an instrument at a Cassegrain focus of a telescope, is required for the aimed polarization accuracy.

5.5.1 Instrumental polarization

Instrumental polarization of imaging polarimetry and spectro-polarimetry was evaluated by observing unpolarized standard stars.[15,16]

An average of the measured instrumental polarization ($q_{\rm inst}, u_{\rm inst}$) and its standard deviation ($\sigma_{\rm q_{inst}}, \sigma_{\rm u_{inst}}$) at various telescope positions and observational epochs for imaging polarimetry are shown in Fig. 12 and Table 5. Between V and H bands, instrumental polarization is at 0.04–0.09 % and stable within 0.04–0.12 %. At B and K_s bands, slightly larger instrumental polarization of $\sim$ 0.2 % with a stability of 0.2–0.3 % is measured.

Fluctuation of instrumental polarization among the field of view is evaluated at R_C and J bands by measuring linear polarization of an unpolarized standard star at different positions on the focal plane. Figure 14 shows the measured instrumental polarization over the field positions. In Table 6, an average of the instrumental polarization over the field of view and its standard deviation among the various positions are shown. At R_C band, instrumental polarization is $\sim$ 0.03 % on average and fluctuates by $\sim$ 0.1 %. At J-band, instrumental polarization is $\sim$ 0.1 % that fluctuates by $\sim$ 0.2 %.

Figure 13 shows instrumental polarization of spectro-polarimetry at three independent observational epochs. Instrumental polarization is small and stable at a level better than 0.05 % in optical wavelengths. At near-infrared wavelengths, the fluctuation among the epochs is a few $\times$ 0.1 %, slightly larger than that at optical wavelengths.

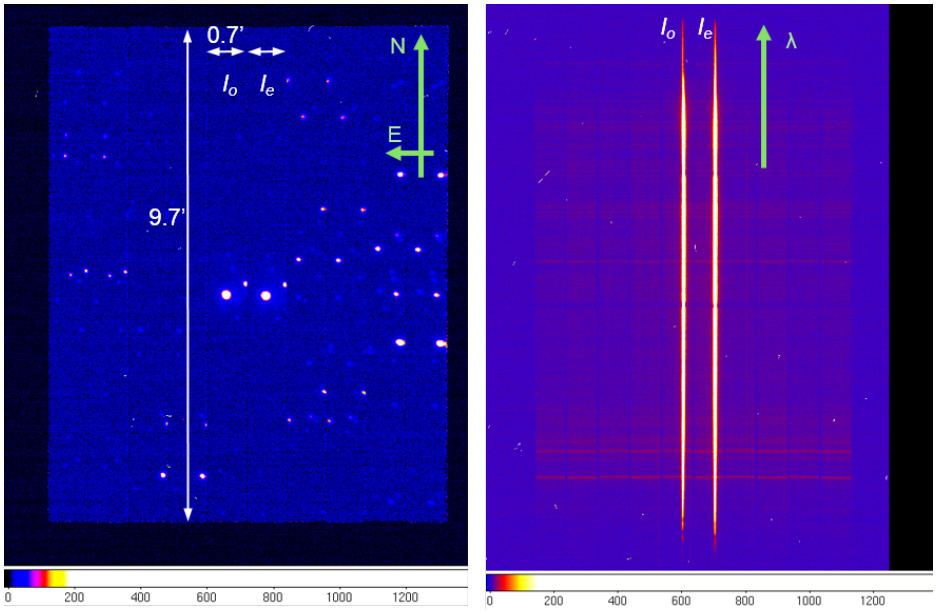

Figure 11. Image samples of imaging polarimetry (left) and spectro-polarimetry (right) on the optical CCD detector.

Table 5. Instrumental polarization of imaging polarimetry.

Band	$\lambda_{\rm center}$[a](μm)	$q_{\rm inst}$ [%]	$u_{\rm inst}$ [%]	$\sigma_{q_{\rm inst}}$ [%]	$\sigma_{u_{\rm inst}}$ [%]	$p_{\rm inst}$[b][%]	$\sigma_{p_{\rm inst}}$[c][%]
B	0.4435	-0.23	0.06	0.21	0.05	0.24	0.22
V	0.5491	-0.01	-0.06	0.02	0.03	0.06	0.04
R_C	0.6534	0.02	-0.06	0.06	0.06	0.06	0.08
I_C	0.7694	-0.03	-0.04	0.03	0.05	0.05	0.06
J	1.2485	-0.09	-0.01	0.09	0.08	0.09	0.12
H	1.6380	0.03	-0.02	0.10	0.03	0.04	0.10
K_s	2.1455	0.10	-0.16	0.22	0.19	0.19	0.29

[a] Central wavelength of the band.
[b] Amplitude of the instrumental polarization; $p_{\rm inst} = \sqrt{q_{\rm inst}^2 + u_{\rm inst}^2}$.
[c] Fluctuation of the instrumental polarization: $\sigma_{p_{\rm inst}} = \sqrt{\sigma_{q_{\rm inst}}^2 + \sigma_{u_{\rm inst}}^2}$.

Table 6. Variation of instrumental polarization in the field of view.

	Average		Standard deviation	
Band	q	u	σ_q	σ_u
R_C	-0.01	-0.03	-0.06	0.08
J	0.08	-0.06	0.09	0.14

5.5.2 Polarization efficiency

We measured polarization efficiency of the optical train by observing a star through a broadband wire-grid linear polarizer (Edumund Optics, Inc.; #68-751; > 1000 contrast at 0.5–3 μm), namely an artificially 100 % polarized star, by imaging polarimetry. Five stars with a color ranging from $B-V \sim 0.0$ to 1.3 were observed. Apparent polarization degrees for the 100 % polarized stars deduced with the formulae in Section 5.4 have a tendency to decrease at shorter wavelengths, reaching about $\sim$ 38 % at B-band. This strong depolarization, especially at the shorter wavelength, is probably due to birefringence of an YLF crystal of the Wollaston prism, by which cross talk between linear polarization and circular polarization occurs.

Observed polarization parameters q, u, and p of a celestial object should be finally divided by the measured polarization efficiency to deduce a real polarization degree of the object. Measured polarization efficiency in each band presents fluctuation due to the color difference of the observed stars ($\sigma_{p_{\rm WG}}$ in Table 7), which causes an error $\epsilon_{\rm pe} = 100(\sigma_{p_{\rm WG}}/p_{\rm WG})$ [%] as a ratio to the observed polarization degree after correcting the

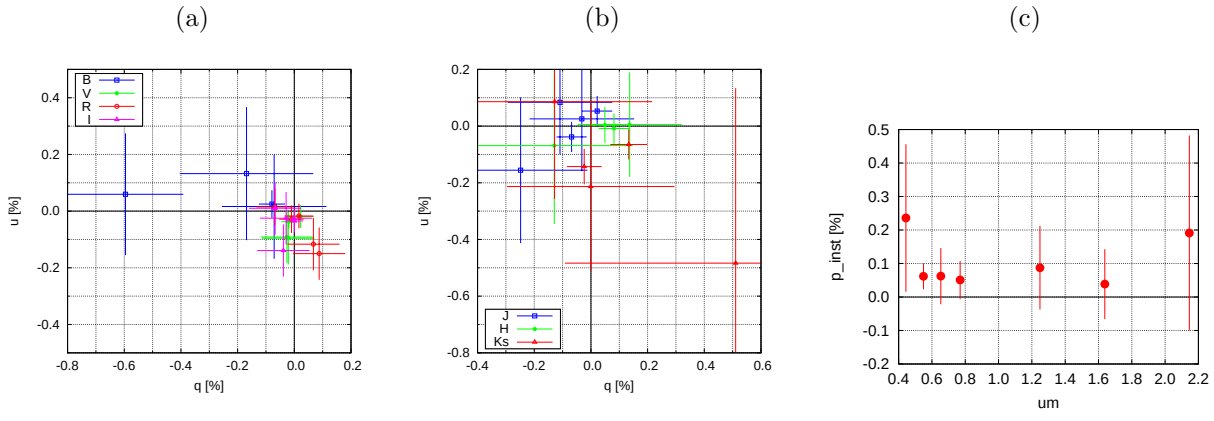

Figure 12. Instrumental polarization and its fluctuation among various telescope positions. (a) Optical bands, and (b) near-infrared bands. (c) Averaged amplitude of the instrumental polarization and its fluctuation (error bars).

polarization efficiency. The error $\epsilon_{\rm pe}$ is 0.2–1.0 % at between R_C and H band, 1.0–1.5 % at V and K_s bands, and ~ 2 % at B band. Actual error by polarization efficiency correction is $\epsilon_{\rm pe}/100 \times p_{\rm obs}$ [%], where $p_{\rm obs}$ [%] is an observed polarization degree of the target object. In almost cases for objects with a polarization degree of a few percent, an error caused by the fluctuation of the polarization efficiency is < 0.1 %.

Polarization efficiency measured by spectro-polarimetry is consistent with that of imaging polarimetry (Fig. 15(a)).

5.5.3 Position angle calibration

A position angle of the optical axis of a super-achromatic half-wave plate varies with wavelength. Figure 15(b) shows observed position angles of a star through a chromatic wire-gird polarizer with a constant position angle of the 100 % linear polarization over the whole of observable wavelengths, by imaging polarimetry and

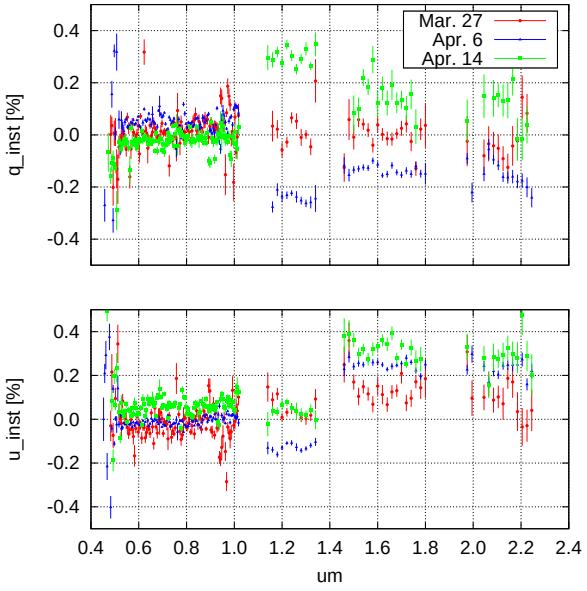

Figure 13. Instrumental polarization of spectro-polarimetry $(q(\lambda), u(\lambda))$ at three epochs.

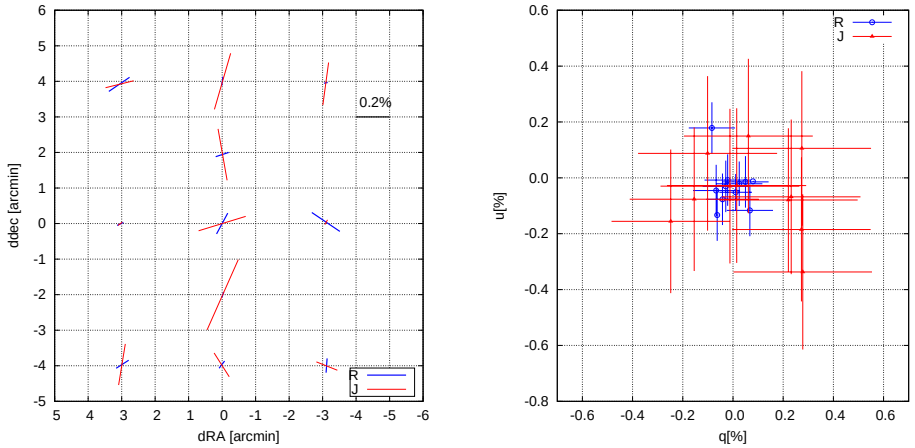

(a) (b)

Figure 14. Fluctuation of instrumental polarization in the field of view. (a) Polarization vectors in the field of view. (b) Distribution of normalized stokes parameters.

.

Table 7. Measured polarization of a star through a wire-grid polarizer.

Band	$\lambda_{\rm center}$ [μm]	$p_{\rm WG}$[a][%]	$\sigma_{p_{\rm WG}}$[a][%]	$\theta_{\rm WG}$[b][degree]	$\sigma_{\theta_{\rm WG}}$[b][degree]	ϵ_{pe}[c][%]
B	0.4435	38.4	0.8	11.1	1.9	2.1
V	0.5491	50.9	0.8	2.3	0.4	1.5
R_C	0.6534	62.6	0.6	0.0	0.0	0.9
I_C	0.7694	73.8	0.5	2.0	0.3	0.7
J	1.2485	88.7	0.2	1.8	0.5	0.3
H	1.6380	93.4	0.1	-1.5	0.5	0.2
K_s	2.1455	96.9	1.1	-3.4	0.5	1.2

[a] An average and standard deviation of measured polarization degrees of various stars through a wire-grid polarizer.
[b] An average and standard deviation of measured position angles of wire-grid stars.
[c] An expected error ratio to an observed polarization degree of a target object after correction of polarization efficiency. $\epsilon_{pe} = 100(\sigma_{p_{\rm WG}}/p_{\rm WG})$.

spectro-polarimetry. Variation of the position angle, caused by the wavelength dependency of the optical axis of the HWP plate, is within 15 degrees and consistent between imaging polarimetry and spectro-polarimetry.

The instrumental position angle against celestial coordinate, which should be corrected for the observed position angle, is determined by measuring polarization position angles of strongly polarized standard stars whose position angle has been known.[15,16] A typical accuracy of determination of the instrumental position angle is within 0°.1.

5.6 Initial results

Figure 16 shows interstellar polarization spectra measured by imaging polarimetry and spectro-polarimetry compared with the previous measurements in the literature.[17]

6. SUMMARY

We have developed an optical and near-infrared simultaneous instrument HONIR since 2007. In addition to the existing imaging capability, we have now introduced spectroscopy and polarimetry capabilities. Every function presents good performance in general with some issues to be improved aside. Much further evaluation of the performance of the instrument and its improvement are in progress.

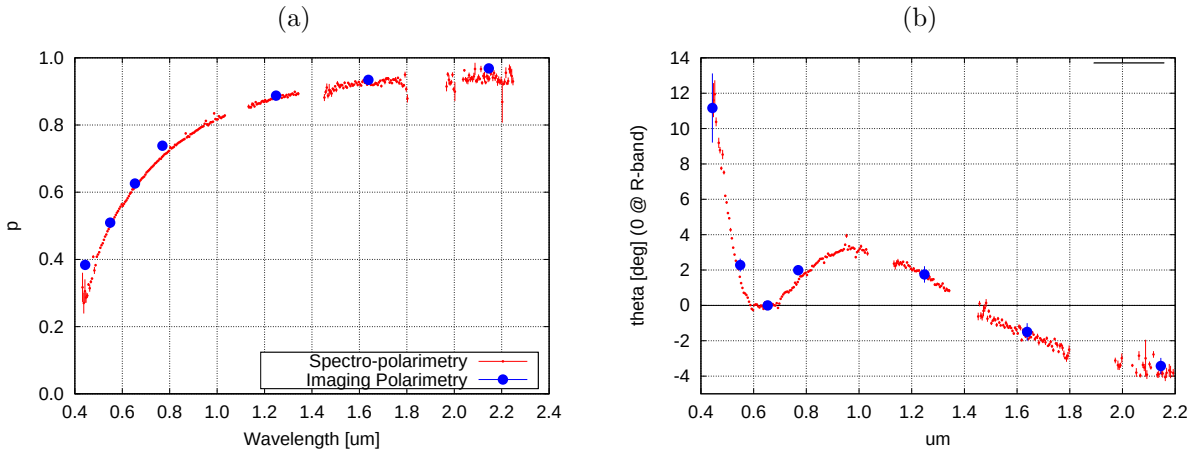

Figure 15. Polarization spectra of a star through a chromatic wire-grid polarizer. (a) Polarization degree and (b) Position angle (relative to R_C-band).

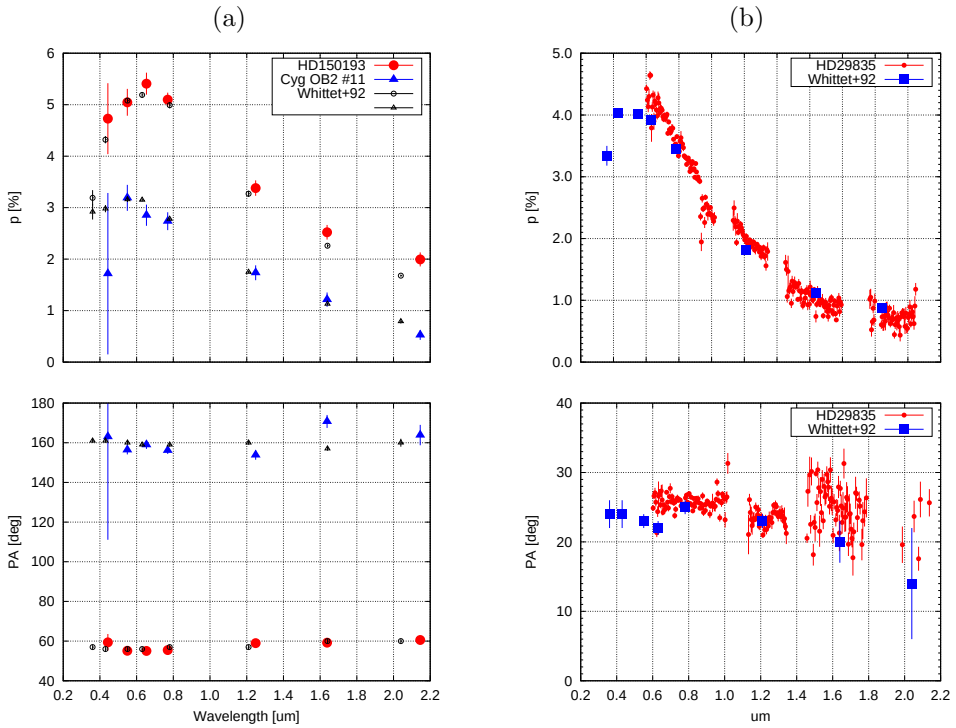

Figure 16. Measured insterstellar polarization spectra by (a) imaging polarimetry and (b) spectro-polarimetry. Previous measurements by Whittet et al.[17] are also shown.

An improved readout system for the HgCdTe VIRGO-2K detector, which achieves a faster readout frame rate, will be in operation[12] in the near future. Installation of an offset guider system and an additional near-infrared arm (IR Arm #2) are also major goals of the development of the instrument.

ACKNOWLEDGMENTS

We are grateful to S. Sato, S. Sako, K. Okita, Y. Hirahara, M. Kino, N. Takahashi, M. Konishi, and K. Yanagisawa for helpful comments and kind cooperation. The development of the instrument has been supported in part by Optical & Near-Infrared Astronomy Inter-University Cooperation Program, supported by the MEXT of Japan. This research has been supported in part by the Grant-in-Aid for Scientific Research (23244030, 23340048, 26287031) from the JSPS and MEXT, Japan. Y.M., R.I., and K.T. are supported through the JSPS (Japan Society for the Promotion of Science) Research Fellowship for Young Scientists. Evaluation of performance of the optical elements was supported by Advanced Technology Center, National Astronomical Observatory of Japan.

REFERENCES

[1] Abdo, A. A., Ackermann, M., Ajello, M., Axelsson, M., Baldini, L., Ballet, J., Barbiellini, G., Bastieri, D., Baughman, B. M., Bechtol, K., and et al., "A change in the optical polarization associated with a γ-ray flare in the blazar 3C279," *Nature* **463**, 919–923 (2010).

[2] Ikejiri, Y., Uemura, M., Sasada, M., Ito, R., Yamanaka, M., Sakimoto, K., Arai, A., Fukazawa, Y., Ohsugi, T., Kawabata, K. S., Yoshida, M., Sato, S., and Kino, M., "Photopolarimetric Monitoring of Blazars in the Optical and Near-Infrared Bands with the Kanata Telescope. I. Correlations between Flux, Color, and Polarization," *Publ. Astron. Soc. Jpn.* **63**, 639–675 (2011).

[3] Sasada, M., Uemura, M., Arai, A., Fukazawa, Y., Kawabata, K. S., Ohsugi, T., Yamashita, T., Isogai, M., Nagae, O., Uehara, T., Mizuno, T., Katagiri, H., Takahashi, H., Sato, S., and Kino, M., "Multiband

Photopolarimetric Monitoring of an Outburst of the Blazar 3C 454.3 in 2007," *Publ. Astron. Soc. Jpn.* **62**, 645–652 (2010).

[4] Yamanaka, M., Kawabata, K. S., Kinugasa, K., Tanaka, M., Imada, A., Maeda, K., Nomoto, K., Arai, A., Chiyonobu, S., Fukazawa, Y., Hashimoto, O., Honda, S., Ikejiri, Y., Itoh, R., Kamata, Y., Kawai, N., Komatsu, T., Konishi, K., Kuroda, D., Miyamoto, H., Miyazaki, S., Nagae, O., Nakaya, H., Ohsugi, T., Omodaka, T., Sakai, N., Sasada, M., Suzuki, M., Taguchi, H., Takahashi, H., Tanaka, H., Uemura, M., Yamashita, T., Yanagisawa, K., and Yoshida, M., "Early Phase Observations of Extremely Luminous Type Ia Supernova 2009dc," *Astrophys. J.* **707**, L118–L122 (2009).

[5] Watanabe, M., Nakaya, H., Yamamuro, T., Zenno, T., Ishii, M., Okada, M., Yamazaki, A., Yamanaka, Y., Kurita, M., Kino, M., Ijiri, R., Hirao, T., Nagata, T., Sato, S., Kawai, T., Nakamura, Y., Sato, T., Ebizuka, N., Hough, J. H., and Chrysostomou, A., "TRISPEC: A Simultaneous Optical and Near-Infrared Imager, Spectrograph, and Polarimeter," *Publ. Astron. Soc. Pac.* **117**, 870–884 (2005).

[6] Sakimoto, K., Akitaya, H., Yamashita, T., Kawabata, K. S., Nakaya, H., Miyamoto, H., Harao, T., Itoh, R., Matsui, R., Moritani, Y., Nakashima, A., Ohsugi, T., Sasada, M., Takaki, K., Ueno, I., Ui, T., Urano, T., and Yoshida, M., "An optical and near-infrared multipurpose instrument HONIR," in [*Society of Photo-Optical Instrumentation Engineers (SPIE) Conference Series*], *Society of Photo-Optical Instrumentation Engineers (SPIE) Conference Series* **8446**, 844673 (Sept. 2012).

[7] Nakaya, H., Komiyama, Y., Miyazaki, S., Yamashita, T., Yagi, M., and Sekiguchi, M., "New Focal Plane Array Controller for the Instruments of the Subaru Telescope," *Publ. Astron. Soc. Pac.* **118**, 478–488 (2006).

[8] Nakaya, H., Doi, Y., Kamata, Y., Komiyama, Y., and Miyazaki, S., "HyperSuprime: electronics," *Proceedings of SPIE* **6269**, 62693G (2006).

[9] Nakaya, H., "CCD Readout Electronics for Subaru Telescope Instruments," *Publ. Astron. Soc. Pac.* **124**, 485–493 (2012).

[10] Nakaya, H. and Sato, S., "Multi-array control system for a wide-wavelength observation," *Proceedings of SPIE* **3354**, 368–372 (1998).

[11] Sako, S., Aoki, T., Doi, M., Ienaka, N., Kobayashi, N., Matsunaga, N., Mito, H., Miyata, T., Morokuma, T., Nakada, Y., Soyano, T., Tarusawa, K., Miyazaki, S., Nakata, F., Okada, N., Sarugaku, Y., and Richmond, M. W., "KWFC: four square degrees camera for the Kiso Schmidt Telescope," in [*Society of Photo-Optical Instrumentation Engineers (SPIE) Conference Series*], *Society of Photo-Optical Instrumentation Engineers (SPIE) Conference Series* **8446**, 84466L (Sept. 2012).

[12] Ui, T., Sako, S., Yamashita, T., Akitaya, H., Kawabata, K. S., Nakaya, H., Moritani, Y., Itoh, R., Takaki, K., Urano, T., Ueno, I., Ohsugi, T., Yoshida, M., Nakao, H., and Hashiba, Y., "Development of a new readout system for the near-infrared detector of HONIR," *Proceedings of SPIE* **9147**, in this conference (2014).

[13] Perrin, M. D., Graham, J. R., and Lloyd, J. P., "The IRCAL Polarimeter: Design, Calibration, and Data Reduction for an Adaptive Optics Imaging Polarimeter," *Publ. Astron. Soc. Pac.* **120**, 555–570 (2008).

[14] Kawabata, K. S., Okazaki, A., Akitaya, H., Hirakata, N., Hirata, R., Ikeda, Y., Kondoh, M., Masuda, S., and Seki, M., "A New Spectropolarimeter at the Dodaira Observatory," *Publ. Astron. Soc. Pac.* **111**, 898–908 (July 1999).

[15] Schmidt, G. D., Elston, R., and Lupie, O. L., "The Hubble Space Telescope Northern-Hemisphere grid of stellar polarimetric standards," *Astron. J.* **104**, 1563–1567 (Oct. 1992).

[16] Turnshek, D. A., Bohlin, R. C., Williamson, II, R. L., Lupie, O. L., Koornneef, J., and Morgan, D. H., "An atlas of Hubble Space Telescope photometric, spectrophotometric, and polarimetric calibration objects," *Astron. J.* **99**, 1243–1261 (Apr. 1990).

[17] Whittet, D. C. B., Martin, P. G., Hough, J. H., Rouse, M. F., Bailey, J. A., and Axon, D. J., "Systematic variations in the wavelength dependence of interstellar linear polarization," *Astrophys. J.* **386**, 562–577 (Feb. 1992).